Twinning Engineering of a CoCrFeMnNi High-Entropy Alloy

Jongun Moon, Olivier Bouaziz, Hyoung Seop Kim, Yuri Estrin

Version of Record: https://www.sciencedirect.com/science/article/pii/S1359646221000889
Manuscript_955dd7a1ae63294fbc1c146976f97dcb

Twinning Engineering of a CoCrFeMnNi High-Entropy Alloy Inspired by Twinning-Induced Plasticity Steels

Jongun Moon[1,2], Olivier Bouaziz[3,4,*], Hyoung Seop Kim[1,2,5,*], Yuri Estrin[6,7]

[1]*Department of Materials Science and Engineering, Pohang University of Science and Technology (POSTECH), Pohang 37673, Republic of Korea*

[2]*Center for High Entropy Alloys, Pohang University of Science and Technology (POSTECH), Pohang 37673, Republic of Korea*

[3]*Laboratoire d'Etude des Microstructures et de Mécanique des Matériaux (LEM3), CNRS, Université de Lorraine, Arts et Métier Paris Tech, F 57000, Metz, France*

[4]*LABoratoire d'EXcellence DAMAS, Université de Lorraine, 57000, Metz, France*

[5]*Graduate Institute for Ferrous Technology, Pohang University of Science and Technology (POSTECH), Pohang 37673, Republic of Korea*

[6]*Department of Materials Science and Engineering, Monash University, Clayton, VIC 3800, Australia*

[7]*Department of Mechanical Engineering, The University of Western Australia, Crawley, WA 6009, Australia*

*Corresponding authors: E-mail address: olivier.bouaziz@univ-lorraine.fr (O. Bouaziz), hskim@postech.ac.kr (H.S. Kim)

Abstract

Deformation-induced twinning has been a notable example of overcoming the strength/ductility trade-off dilemma as a strengthening mechanism. By borrowing this concept from the area of TWIP steels, we designed a thermomechanical treatment for a CoCrFeMnNi high-entropy alloy to improve its mechanical characteristics. We used pre-straining at 77 K to introduce deformation-induced twins in the microstructure of the alloy, and then recovered it by annealing at 773 K, while avoiding recrystallization. The deformation-induced twins generated by pre-straining at 77 K were retained after this heat treatment, whilst partial recovery of dislocations occurred. As a result, the room-temperature mechanical properties of the alloy, including its strain hardening ability, were improved substantially.

Keywords: high-entropy alloys, twinning, recovery, strain hardening, ductility

Deformation-induced twins (DTs) are known to act as strong obstacles to moving dislocations [1, 2]. Sustained deformation twinning in high manganese twinning-induced plasticity (TWIP) steels gives rise to a continual reduction of the mean free path of dislocations, thus enabling strain hardening and promoting high ductility [3-5]. This profuse twinning promoted by a favourable magnitude of the stacking fault energy (SFE) enables the TWIP steels to possess substantial strain hardening at room temperature (RT) [1, 2]. Moreover, deformation-induced twins in TWIP steels were found to be thermally stable up to ~898 K [6]. Building on this thermal stability of DTs, some ten years ago a metallurgical route was proposed to improve the yield strength of TWIP steels [7]. It encompasses the following steps: First, pre-straining is applied at RT to generate deformation-induced twins. This is followed by annealing at 773 K with the aim to reduce the dislocation density by static recovery, while sustaining the DTs due to their thermal stability being higher than that of the dislocations. Through this 'twinning engineering', a favourable combination of high yield strength and enhanced uniform elongation of TWIP steels was achieved [7].

An exciting development in materials engineering has been the advent of a novel class of materials, which comprise multiple principal elements in a high concentration and are referred to as high-entropy alloys (HEAs) [8-10]. They were developed in the 1970s, but came to the fore in the last decade due to their exceptional mechanical characteristics [11]. Specifically, face-centered cubic (FCC) HEAs exhibit outstanding mechanical properties in the temperature range from cryogenic [12-14] to ambient [15-18] temperatures. The mechanisms underlying these properties are associated with the deformation-induced twinning [12, 15] and/or phase transformations [13, 14]. Among the FCC-based HEAs, the now classical Cantor alloy CoCrFeMnNi exhibits deformation-induced twinning at 77 K, resulting in outstanding tensile properties along with a high fracture toughness [12]. Using this feature, Sun *et al.* [19, 20] demonstrated that the yield strength of the CoCrFeMnNi HEA

at RT is enhanced by pre-straining at 77 K. No annealing heat treatment was involved in their work.

In the present communication, we propose a way to improve the tensile properties of the Cantor alloy even further. The novelty of this work consists in translating the strategy based on the thermomechanical route (pre-straining and recovery), which has been so successful for TWIP steels, to a high-entropy alloy. The results of a systematic investigation of the mechanical properties and microstructure evolution of an equiatomic CoCrFeMnNi alloy at RT after pre-straining at 77 K followed by an annealing treatment are reported below.

An ingot of a HEA $Co_{20}Cr_{20}Fe_{20}Mn_{20}Ni_{20}$ (atomic percent, at%) was fabricated using vacuum induction melting in argon atmosphere. The ingot was homogenized at 1,373 K for 6 h in argon atmosphere, followed by water quenching. The surface of the homogenized ingot was mechanically milled in order to reduce surface roughness and remove oxides. After this preparation, cold rolling with a thickness reduction from 7 mm to 1.5 mm was performed. The cold-rolled plate was annealed at 1073 K for 1 h in argon atmosphere to achieve full recrystallization [21], followed by water quenching.

From this plate, dog-bone shaped tensile specimens with a gauge length of 5 mm and a width of 2.5 mm were cut. All tensile tests were conducted on an Instron 1361 machine. The deformation curves for the annealed alloy measured at RT and 77 K are presented in Fig. 1(a). In addition to continuous tests to failure, the annealed alloy was deformed at 77 K to different strains, 20%, 35%, and 50%, as shown in Fig. 1(b). After straining at 77 K, the specimens were heat treated at 773 K for 1 h in argon atmosphere, followed by water quenching. Henceforth, the specimens with different processing histories are referred to as P20, P35, P50, P20 + HT, P35 + HT, and P50 + HT, according to the strain to which they were deformed at 77 K and the recovery heat treatment. The processing histories and nomenclature used in the present work are summarized in Table 1. Before the tensile tests, the specimens were polished using SiC papers up to 1200-grit. All tensile tests, including pre-straining at 77 K, were performed at a strain rate of 10^{-3} s^{-1}. An extensometer was attached to the gauge section of each specimen to measure the engineering strain during the tests.

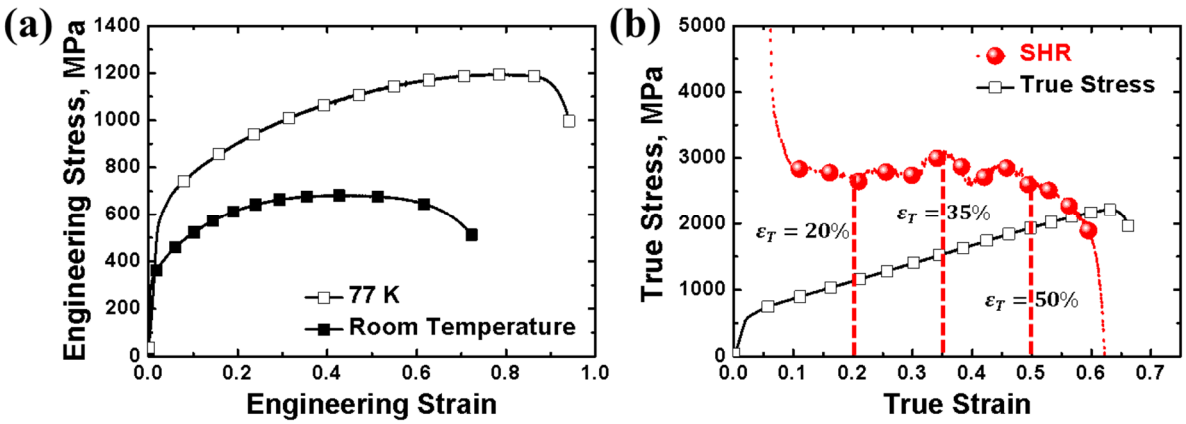

Figure 1. (a) Engineering stress-strain curves at room temperature and 77 K. (b) The true stress vs. true strain curve for a specimen pre-strained at 77 K. The corresponding variation of the strain hardening rate (SHR) with true strain is shown in red. The selected values of the low-temperature pre-strain and the attendant levels of the SHR are indicated by the vertical dash lines.

Table 1. The $Co_{20}Cr_{20}Fe_{20}Mn_{20}Ni_{20}$ alloy with the different processing histories.

Processing histories	Naming
Pre-straining to a true strain of 20% at 77 K	P20
Pre-straining to a true strain of 35% at 77 K	P35
Pre-straining to a true strain of 50% at 77 K	P50
Pre-straining to a true strain of 20% at 77 K + recovery heat treatment at 773 K for 1 h	P20 + HT
Pre-straining to a true strain of 35% at 77 K + recovery heat treatment at 773 K for 1 h	P35 + HT
Pre-straining to a true strain of 50% at 77 K + recovery heat treatment at 773 K for 1 h	P50 + HT

Scanning electron microscopy (SEM) with electron backscatter diffraction (EBSD) was performed using a JEOL 7800F device and TSL/OIM software. EBSD measurements were conducted with a step size of 50 nm. The surface of the alloy for SEM/EBSD characterization was polished up to 1200-grit SiC paper, followed by electro-polishing in an etchant solution of 8% perchloric acid.

Figure 2 shows the kernel average misorientation (KAM) maps and its distribution for the specimens with different processing histories. The KAM values revealed through the maps [Figs. 2(a, b, d, e, g, h)] and the corresponding distribution plots [Figs. 2(c, f, i)] demonstrate that the deformation applied by pre-straining was relieved as a result of the recovery heat treatment. Notably, the average KAM (KAM_{avg}) values of the pre-strained specimens decline from 1.63° to 1.19° (P20), 2.23° to 1.65° (P35), and 2.31° to 1.77° (P50) after heat treatment.

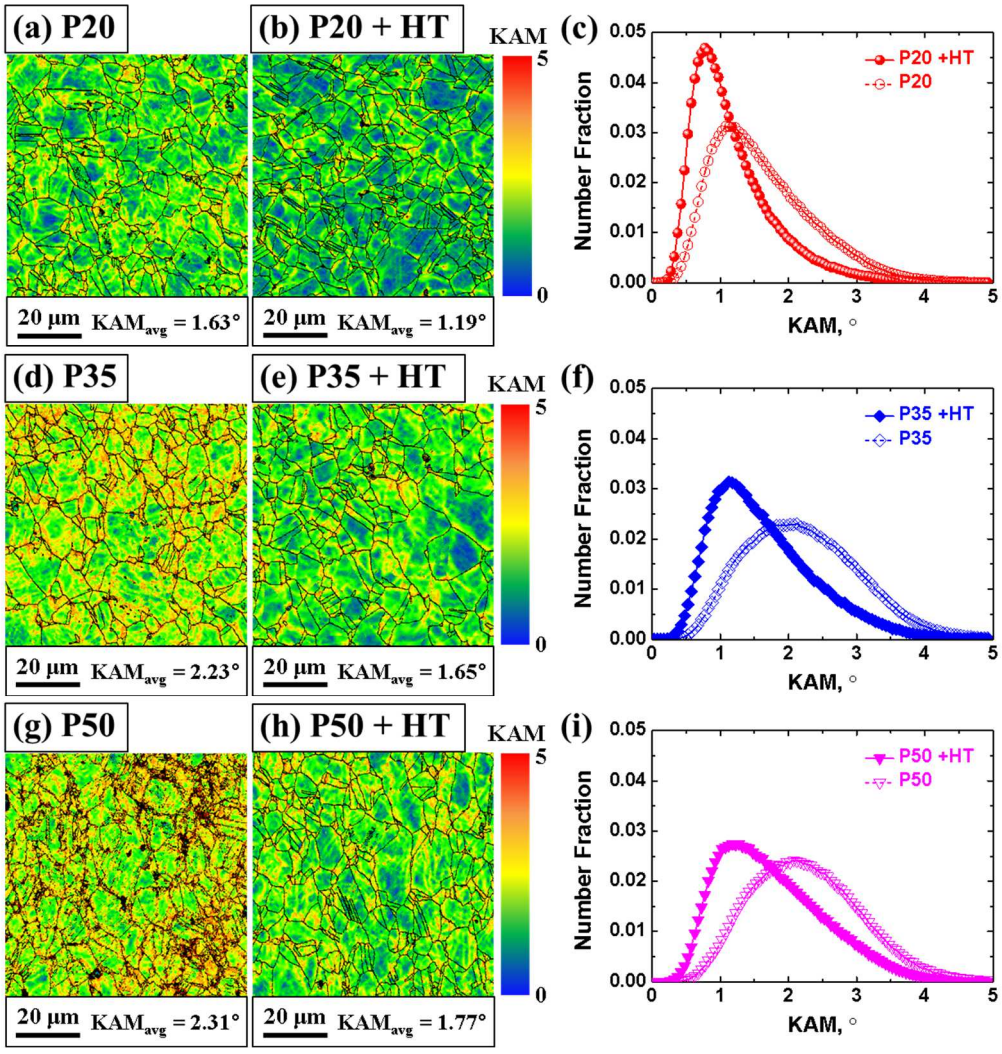

Figure 2. EBSD KAM maps and the corresponding distribution plots for the pre-strained specimens before and after recovery heat treatment: (a-c) P20 and P20 + HT, (d-f) P35 and P35 + HT, and (g-i) P50 and P50 + HT, respectively.

The microstructures of the annealed, P20 + HT, P35 + HT, and P50 + HT specimens, showing grain and twin boundaries, are presented in Fig. 3. The average grain size of the fully recrystallized annealed alloy is 11.54 $\pm$ 4.19 μm, while that after the pre-straining is ~8 μm. Although the grains are elongated along the tensile direction after the pre-straining and heat treatment, the change in grain size is negligible. In the annealed alloy, profuse annealing twins (AT) are observed [Fig. 3(a)]. The areal fraction of twins increases from 19.55% in the annealed state to 21.38% (P20 + HT), 23.50% (P35 + HT), and 25.54% (P50 + HT) as the low-temperature pre-strain increases [Figs. 3(b-d)]. The increasing fraction of twins in the heat treated alloy indicates that the DTs formed as a result of pre-straining at 77 K sustained after the heat treatment, while dislocations are recovered as shown in Fig. 2. The area fraction of the retained DTs (V_{RDT}) as a function of the pre-strain is presented in Fig. 3(e). It was determined by subtracting the fraction of annealing twins (ATs) from the total fraction of twins, without distinction of their provenance. As the applied pre-strain increases, the fraction of deformation-induced twins, V_{DT}, is seen to increase monotonically, which is consistent with the results of an earlier work [22].

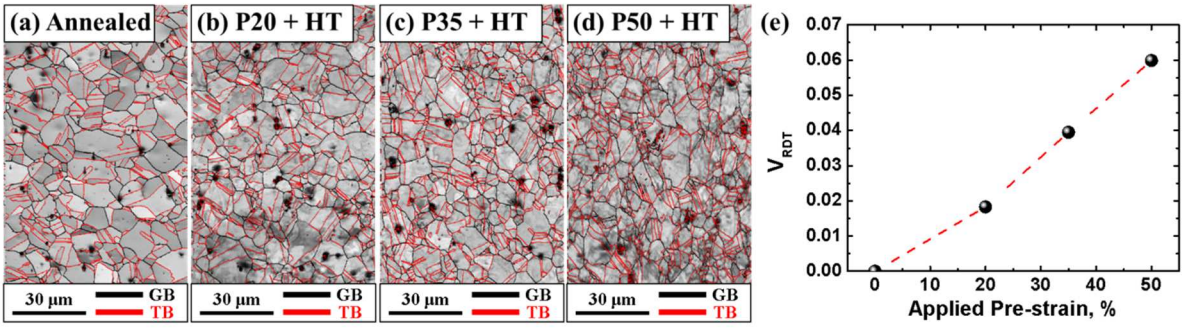

Figure 3. EBSD image quality maps of (a) annealed, (b) P20 + HT, (c) P35 + HT, and (d) P50 + HT alloys. The black and red lines in (a-d) represent grain boundary (GB) and twin boundary (TB), respectively. (e) V_{DT} as a function of applied pre-strain at 77 K.

Mechanical behavior of the alloy after the different thermomechanical routes is shown in Fig. 4. The yield strength and the ultimate tensile strength increase from 309 MPa and 683 MPa in the annealed state to 819 MPa and 890 MPa (P20 + HT), 1,033 MPa and 1,040 MPa (P35 + HT), and 1,284 MPa and 1,297 MPa (P50 + HT) for the different schedules of thermomechanical processing, respectively [Fig. 4(a)]. The uniform elongation also varies monotonically, dropping from 43% in the annealed condition to 18% (P20 + HT), 8% (P35 + HT), and 1% (P50 + HT) with growing pre-strain. The combination of the yield strength and the uniform elongation after the heat treatment appears to be particularly good for the P20 + HT and P35 + HT alloys – similar to the results for TWIP steels [7]. This demonstrates that the thermomechanical processing strategy adopted from TWIP research also works for HEAs. As anticipated, the DTs retained after this processing enhance the yield strength of the alloy. At the same time, the ability of the dislocation density to increase from a low base established by the recovery equips the material with a significant SHR capability, which ensures good tensile ductility [Fig. 4(b)]. Effectively, the SHR of the heat-treated alloy is higher than that of the initially annealed alloy when the cumulative strain accounting for the pre-strain is considered. This becomes evident when the true stress-strain curves at RT are juxtaposed so that a shift by the amount of the pre-strain at 77 K is made [Fig. 4(c)]. Figure 4(d) shows the SHR as a function of true stress, revealing a better trade-off between the stress and the SHR of the alloy recovered by the heat treatment compared to the annealed alloy. It should also be noted that at a fixed SHR level (set at 3,000 MPa) the true flow stress increases with the pre-strain, starting from 484 MPa for the annealed alloy and attaining the values of 833 MPa, 1,040 MPa, and 1,301 MPa for P20 +HT, P35 + HT, and P50 + HT, respectively [Fig. 4(d))].

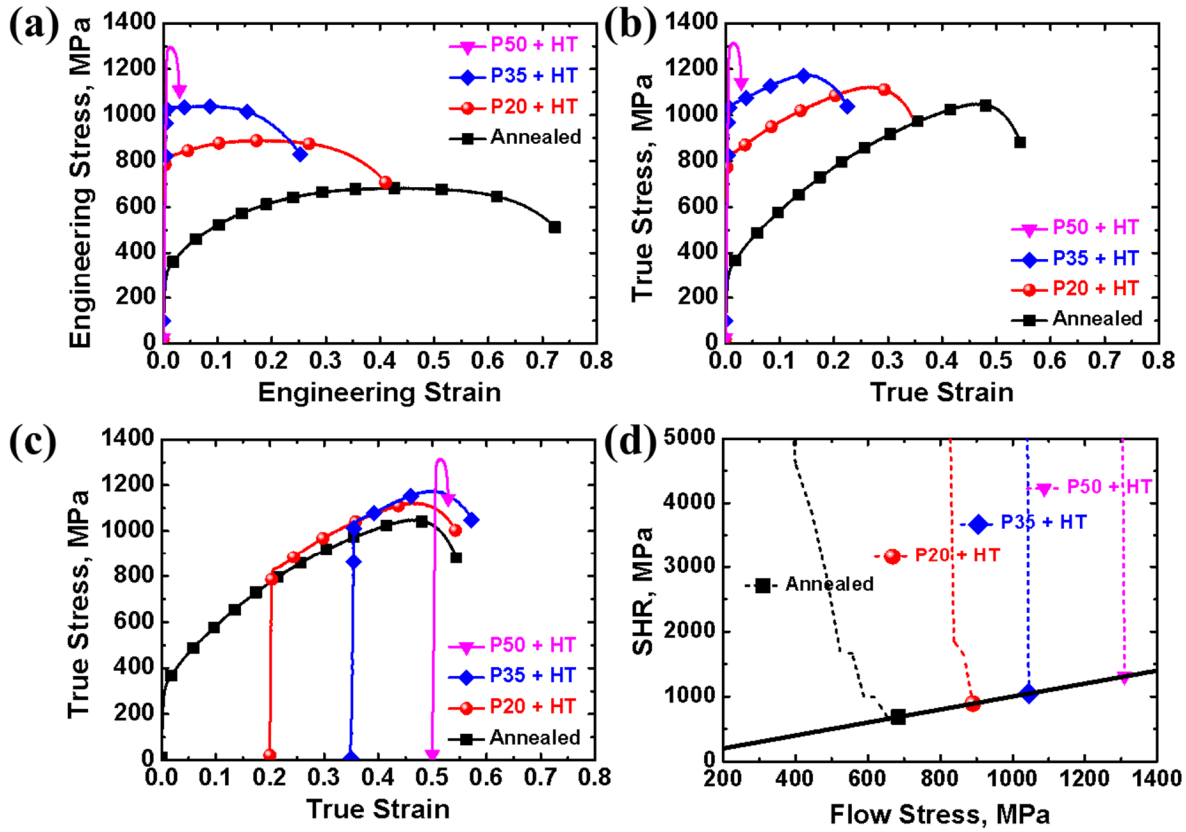

Figure 4. (a) Engineering and (b) true stress-strain curves of the annealed, P20 + HT, P35 + HT, and P50 + HT alloys at room temperature. (c) Juxtaposition of the curves from (b) shifted along the abscissa by the amount of the pre-strain at 77 K. (d) SHR as a function of the true stress for the samples of the alloy with the different thermomechanical histories. The solid black line in (d) corresponds to the Considère criterion.

The yield strength (σ_{YS}) of the present alloy after the different processing routes can be described as follows:

$$\sigma_{YS} = \sigma_0 + \sigma_{GB} + \sigma_{RDT} + \sigma_D, \quad (1)$$

where σ_0 is the lattice friction and σ_{GB}, σ_{RDT}, and σ_D denote the contributions associated with grain boundaries, retained DTs, and dislocations, respectively. Since the variability of the grain size among the samples with different processing histories is insignificant, the change in

σ_{GB} before and after pre-straining can be neglected. Thus, the increment of the yield strength σ_{YS} of the alloy after the thermomechanical processing can be written as:

$$\Delta\sigma_{YS} = \Delta\sigma_{RDT} + \Delta\sigma_{D}. \quad (2)$$

Therefore, the enhancement of σ_{YS} may be associated with the retained DTs and the dislocation density affected by the thermomechanical processing. We can surmise that the dislocation-related effect will enter the yield strength directly, via the Taylor relation

$$\Delta\sigma_{D} = M\alpha Gb\rho^{1/2}, \quad (3)$$

where $M$is the texture-dependent Taylor factor, G is the shear modulus, b is the magnitude of the dislocation Burgers vector, ρ is the dislocation density acquired after the thermomechanical treatment, and α is a numerical constant. By contrast, the effect of the retained twins is indirect: it comes to bearing through enhanced accumulation of the dislocation density due to the presence of the twins, leading to a higher strain hardening rate. Indeed, the mean free path of dislocations (l) can be expressed by the following equation [23]:

$$\frac{1}{l} = \frac{1}{d} + \frac{1}{\lambda}, \quad (4)$$

where d and λ are the average grain size and the twin spacing, respectively. The retained DTs reduce the mean free path of mobile dislocations, leading to a faster rate of dislocation density accumulation, according to the equation [24]:

$$\frac{d\rho}{d\varepsilon} = M\left[\frac{1}{bl} - k_2\rho\right], \quad (5)$$

where k_2 is a dynamic dislocation recovery coefficient. Obviously, a smaller effective mean free path at the beginning of the RT deformation owing to low-temperature pre-straining, and a further decrease of l due to additional twinning during RT straining, lead to a higher SHR than in the annealed material.

Figure 5 shows a comparison of the yield strength of CoCrFeMnNi with respect to the grain size. The yield strength of the alloy reported previously follows the classical Hall-Petch relation [25]:

$$\Delta\sigma_{GB} = \sigma_0 + kd^{-1/2}, \tag{6}$$

where σ_0, k, and d are the lattice friction (125 MPa [26]), the Hall-Petch strengthening coefficient (494 MPa·μm$^{-1/2}$ [26]), and the average grain size, respectively. Some data reported for the CoCrFeMnNi alloy slightly deviate from the Hall-Petch trend, and this may be associated with the high dislocation density and/or DTs induced by pre-straining [20] and high-pressure torsion (HPT) [28]. By contrast, the pre-strained and annealed material investigated in the present work outperforms the conventional grain boundary-strengthened alloys quite remarkably. As seen in Fig. 4(c), the yield strength of the pre-strained and recovered specimens exceeds the flow stress of the annealed specimens attained at the same strain levels. Since the heat treatment causes partial recovery of dislocations (Fig. 2), it can be surmised that the enhancement of the yield strength observed is associated with the retained boundaries of DTs.

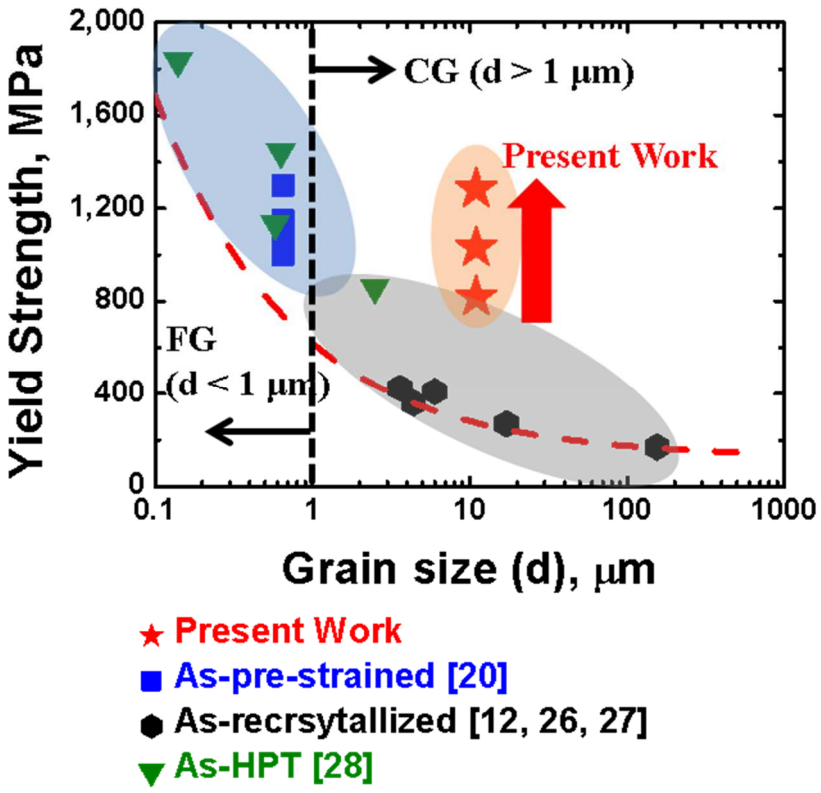

Figure 5. Room-temperature yield strength versus grain size of the present and the previously reported CoCrFeMnNi alloy. CG and FG stand for coarse and fine grains, respectively. The red dashed line represents the Hall-Petch relation for the CoCrFeMnNi alloy established in Ref. [26].

Although the present thermomechanical processing enhances the yield strength and SHR of the alloy, its tensile elongation is not improved sufficiently (Fig. 4). The latter observation can be attributed to partial recovery of dislocations as a result of the heat treatment (Figs. 2(b, e, h)). Despite the partial recovery, the annealed material still contains a considerable dislocation density. This leads to accumulation of mobile dislocations at localized obstacles, which imparts negatively on the ductility of the alloy. A more in-depth study is needed for finding an optimum condition of recovery heat treatment providing an improvement of both strength and ductility characteristics of the alloy. In such a recovery heat

treatment, recrystallization is to be avoided and the DT density maintained, along with a sizeable reduction of the dislocation density.

There are reasons to believe that the success of the twinning engineering approach as applied to the equiatomic HEA CoCrFeMnNi is not fortuitious and can be utilized for other HEAs as well. Indeed, the propensity to deformation twinning that was so crucial in this approach is predicated on the low magnitude of their stacking-fault energy. [29].This feature is quite common to multicomponent HEAs with an equiatomic or nearly equiatomic ratio. It has been reported that they may exhibit local chemical ordering and/or clustering, which influence intrinsic and extrinsic SFEs [29, 30]. A broad range of compositional space in HEAs facilitates alloy design to tune their composition for lowering the SFE intrinsically through local chemical fluctuations, thus promoting deformation twinning [29]. Hence, it can be anticipated that the processing strategy proposed here can be successfully emulated for other high-entropy alloy systems.

In summary, the mechanical properties and microstructural evolution of the equiatomic HEA $Co_{20}Cr_{20}Fe_{20}Mn_{20}Ni_{20}$ subjected to a specially designed thermomechanical treatment, *viz.* pre-straining at 77 K and annealing at 773 K, were investigated systematically, inspired by the metallurgical route developed earlier for TWIP steels. The following conclusions can be drawn:

- The deformation-induced twins introduced by deformation at 77 K are retained during heat treatment at 773 K, while part of dislocations is recovered.
- The remnant deformation-induced twins give rise to an increase of the yield strength and the ultimate tensile strength of the alloy to 1,284 MPa and 1,297 MPa, respectively, with a substantial strain hardening rate at room temperature. These excellent mechanical properties are attributed to a reduction in the mean free path of dislocations by the deformation-induced twins formed by pre-straining at 77 K.
- The ductility of the alloy improves because the remnant deformation-induced twins act to raise the accumulation of dislocations. However, the increase of the tensile elongation attained is moderate, as a sizeable dislocation density survives the recovery heat treatment, which limits the strain hardening capability of the alloy.
- We believe that the two-step thermomechanical treatment strategy developed here for a particular high-entropy alloy, $Co_{20}Cr_{20}Fe_{20}Mn_{20}Ni_{20}$, can be further fine-tuned to increase the gain in properties. We also expect that this processing concept will be applicable to a broader range of HEAs.

Acknowledgments

This work was supported by Creative Materials Discovery Program through the National Research Foundation of Korea (NRF) funded by Ministry of Science and ICT (2016M3D1A1023384).

Declarations of Interest

None.

References

[1] O. Bouaziz, S. Allain, C. Scott, P. Cugy, D. Barbier, *Curr. Opin. Solid State Mater. Sci.* **15** (2011) 141-168.

[2] B. C. De Cooman, O. Kwon, K.-G. Chin, *Mater. Sci. Technol.* **28** (2012), 513-527.

[3] B. C. De Cooman, Y. Estrin, S. K. Kim, *Acta Mater.* **142** (2018) 283-362.

[4] J.-K. Hwang, *Met. Mater. Int.* **26** (2020) 603-616.

[5] M. Park, M. S. Kang, S.-W. Park, H. C. Kim, H.-S. Moon, B. Kim, J. B. Jeon, H. Kim, H.-S. Park, S.-H. Kwon, B. J. Kim, *Met. Mater. Int.* (2020) in press, https://doi.org/10.1007/s12540-020-00785-8.

[6] O. Bouaziz, C. P. Scott, G. Petitgand, *Scripta Mater.* **60** (2009) 714-716.

[7] O. Bouaziz, D. Barbier, P. Cugy, G. Petigand, *Adv. Eng. Mater.* **14** (2012) 49-51.

[8] E. P. George, D. Raabe, R. O. Ritchie, *Nat. Rev. Mater.* **4** (2019) 515-534.

[9] B. Cantor, I. T. H. Chang, P. Knight, A. J. B. Vincent, *Mater. Sci. Eng. A* **375-377** (2004) 213-218.

[10] J.-W. Yeh, S.-K. Chen, S.-J. Lin, J.-Y. Gan, T.-S. Chin, T.-T. Shun, C.-T. Tsau, S.-Y. Chang, *Adv. Eng. Mater.* **6** (2004) 299-303.

[11] B.Cantor, *Prog. Mater. Sci.* (2020) in press, https://doi.org/10.1016/j.pmatsci.2020.100754.

[12] B. Gludovatz, A. Hohenwarter, D. Catoor, E. H. Chang, E. P. George, R. O. Ritchie, *Science* **345** (2014) 1153-1158.

[13] J. Moon, J. M. Park, J. W. Bae, N. Kang, J. Oh, H. Shin, H. S. Kim, *Scripta Mater.* **186** (2020) 24-28.

[14] J. W. Bae, J. B. Seol, J. Moon, S. S. Sohn, M. J. Jang, H. Y. Um, B.-J. Lee, H. S. Kim, *Acta Mater.* **161** (2018) 388-399.

[15] Y. Deng, C. C. Tasan, K. G. Pradeep, H. Springer, A. Kostka, D. Raabe, *Acta Mater.* **94** (2015) 124-133.

[16] J. Moon, J. M. Park, J. W. Bae, H.-S. Do, B.-J. Lee, H. S. Kim, *Acta Mater.* **193** (2020) 71-82.

[17] S.-H. Joo, J. W. Bae, W.-Y. Park, Y. Shimada, T. Wada, H. S. Kim, A. Takeuchi, T. J. Konno, H. Kato, I. V. Okulov, *Adv. Mater.* **32** (2020) 1906160.

[18] H. Gasan, A. Ozcan, *Met. Mater. Int.* **26** (2020) 1152-1167.

[19] S. J. Sun, Y. Z. Tian, H. R. Lin, S. Lu, H. J. Yang, Z. F. Zhang, *Scripta Mater.* **163** (2019) 111-115.

[20] S. J. Sun, Y. Z. Tian, H. R. Lin, Z. J. Wang, Z. F. Zhang, *Mater. Sci. Eng. A* **801** (2021) 140398.

[21] O. Bouaziz, J. Moon, H. S. Kim, Y. Estrin, *Scripta Mater.* **191** (2021) 107-110.

[22] G. Laplanche, A. Kostka, O. M. Horst, G. Eggeler, E. P. George, *Acta Mater.* **118** (2016) 152-163.

[23] O. Bouaziz, N. Guelton, *Mater. Sci. Eng. A* **319-321** (2001) 246-249.

[24] Y. Estrin, H. Mecking, *Acta Mater.* **32** (1984) 57-70.

[25] E. Hall, *Proc. Phys. Soc. B* **64** (1951) 747-753.

[26] F. Otto, A. Dlouhý, Ch. Somsen, H. Bei, G. Eggeler, E. P. George, *Acta Mater.* **61** (2013) 5743-5755.

[27] S. Zherebtsov, N. Stepanov, Y. Ivanisenko, D. Shaysultanov, N. Yurchenko, M. Klimova, G. Salishchev, *Metals* **8** (2018) 123.

[28] M. V. Klimova, D. G. Shaysultanov, S. V. Zherebtsov, N. D. Stepanov, *Mater. Sci. Eng. A* **748** (2019) 228-235.

[29] I. Basu, J. Th. M. De Hosson, *Scripta Mater.* **187** (2020) 148-156.

[30] K. Biswas, J.-W. Yeh, P. P. Bhattacharjee, J. Th. M. De Hosson, *Scripta Mater.* **188** (2020) 54-58.

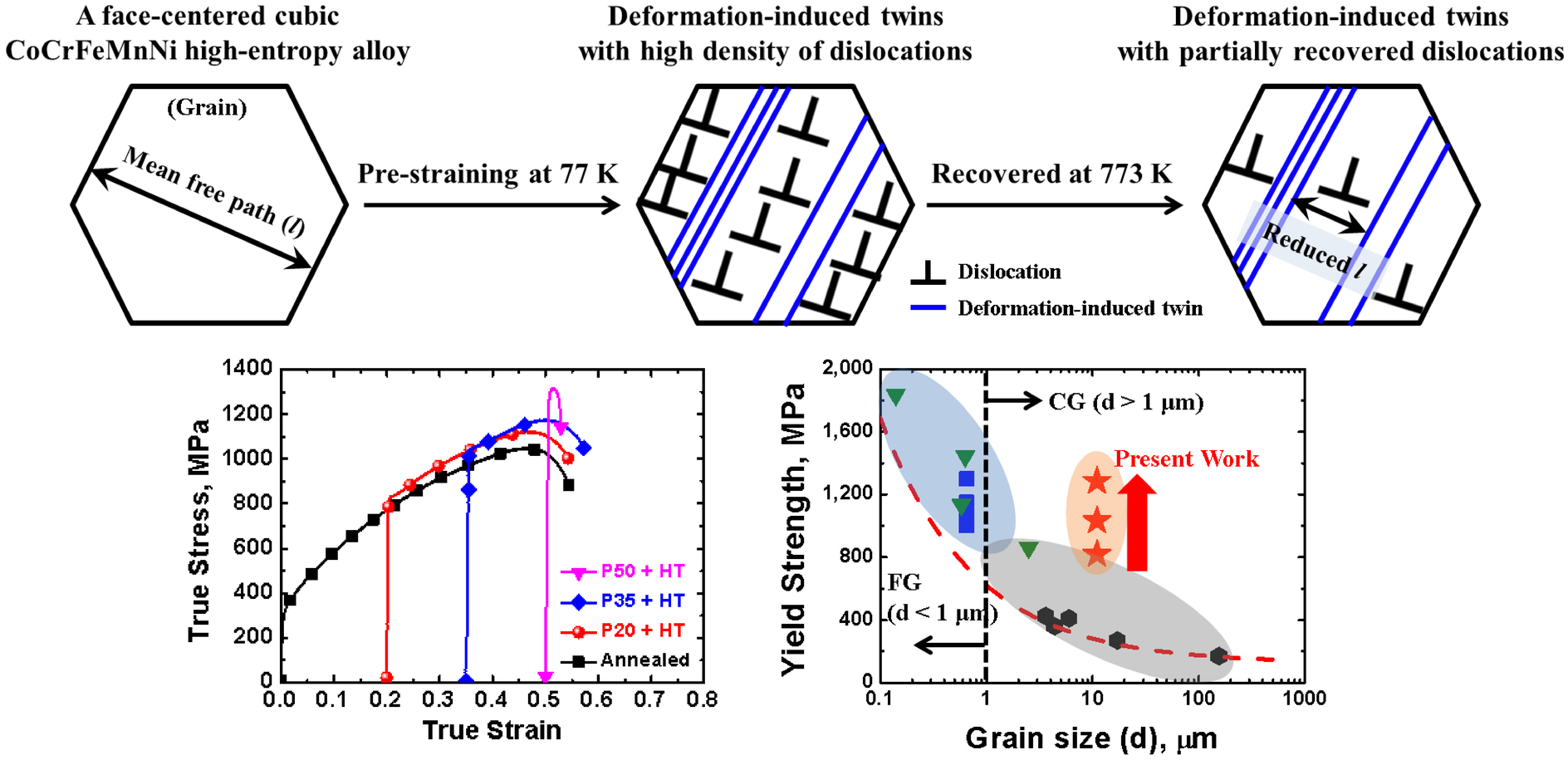
A face-centered cubic
CoCrFeMnNi high-entropy alloy
Deformation-induced twins
with high density of dislocations
Deformation-induced twins
with partially recovered dislocations
(Grain)
Mean free path (l)
Pre-straining at 77 K
Recovered at 773 K
Reduced l
Dislocation
Deformation-induced twin
True Stress, MPa
True Strain
P50 + HT
P35 + HT
P20 + HT
Annealed
Yield Strength, MPa
Grain size (d), μm
CG (d > 1 μm)
FG
(d < 1 μm)
Present Work